ROYAL SOCIETY OF CHEMISTRY

PAPER

Check for updates

Symmetry-breaking charge transfer and intersystem crossing in copper phthalocyanine thin films†

Esther del Pino Rosendo,[a] Okan Yildiz,[a] Wojciech Pisula, [iD] [ab] Tomasz Marszalek,[ab] Paul W. M. Blom [iD] [a] and Charusheela Ramanan [iD] *[ac]

Intermolecular interactions in π-stacked chromophores strongly influence their photophysical properties, and thereby also their function in photonic applications. Mixed electronic and vibrational coupling interactions lead to complex potential energy landscapes with competitive photophysical pathways. Here, we characterize the photoexcited dynamics of the small molecule semiconductor copper pthalocyanine (CuPc) in solution and in thin film, the latter comprising two different π-stacked architectures, α-CuPc and β-CuPc. In solution, CuPc undergoes ultrafast intersytem crossing (ISC) to the triplet excited state. In the solid state, both α-CuPc and β-CuPc morphologies exhibit a mixing between Frenkel and charge-transfer excitons (Frenkel–CT mixing). We find that this mixing influences the photophysical properties differently, based on morphology. In addition to ISC, α-CuPc demonstrates symmetry-breaking charge transfer, which furthermore depends on excitation wavelength. This mechanism is not observed in β-CuPc. These results elucidate how molecular organization mediates the balance of competitive photexcited decay mechanisms in organic semiconductors.

Introduction

Organic semiconductors (OSCs) are being studied and utilized for a broad range of applications, including solar electricity,[1,2] solar fuel production,[3,4] light-emitting diodes,[5–7] and transistors.[8,9] The π-conjugated core or backbone of these materials imparts attractive light-absorption and semiconducting properties. In the thin films often used for optoelectronics, these molecules form aggregates or crystalline structures based on the π-stacking interactions, which can have a significant impact on functional properties.[10–12] Neighboring molecules experience electronic and vibrational coupling interactions that determine their photoactive energy landscape and mediate processes such as light-harvesting, charge separation, and charge transport.

Earlier works established a molecular exciton model for understanding how chromophore packing impacts absorption properties through Coulombic coupling interactions.[13–17] More recently, this model is being extended to consider the significant wavefunction overlap afforded in tightly packed (~ 3.5 Å) π-stacking arrangements, which can allow for short-range charge-transfer (CT) interactions as well.[18–23] These intermolecular CT interactions can furthermore mix with the local intramolecular Frenkel excitons, modifying the potential energy landscape, and thereby also light harvesting, and charge transport properties. Frenkel–CT mixing has been observed in various π-stacked organic chromophore systems, including pentacene,[21,24–27] perylene derivatives,[28–33] squaraines,[34,35] and also in phthalocyanines.[7,36–44] This mixing has been purported to influence photophysical mechanisms, such as singlet fission and the formation of free charge carriers *via* symmetry-breaking charge separation.[26,37]

Copper phthalocyanine (CuPc) is a robust small molecule OSC which, along with related derivatives, has attracted attention for a variety of applications. In addition to being one of the most commonly used pigments for printing blue ink,[45–47] its semiconducting properties make it attractive for optoelectronics and other light-driven applications. CuPc has been used for organic photovoltaics,[1,48–53] light-emitting diodes,[54,55] photodetectors,[56,57] non-linear optics, photocatalysis,[58,59] and photodynamic therapies.[60–62] In thin films, CuPc organizes into different crystalline morphologies depending on the processing conditions. The two most common structures are α-CuPc and

[a] *Max Planck Institute for Polymer Research, Ackermannweg 10, 55128 Mainz, DE, Germany*

[b] *Department of Molecular Physics, Faculty of Chemistry, Lodz University of Technology, Zeromskiego 116, 90-924 Lodz, Poland*

[c] *Department of Physics and Astronomy, Faculty of Sciences, Vrije Universiteit Amsterdam, De Boelelaan 1081, 1081 HV Amsterdam, The Netherlands. E-mail: c.ramanan@vu.nl*

† Electronic supplementary information (ESI) available: Details of excitation density calculations, heating lineshape, additional spectral traces, and DADS comparison. See DOI: https://doi.org/10.1039/d2cp05240g
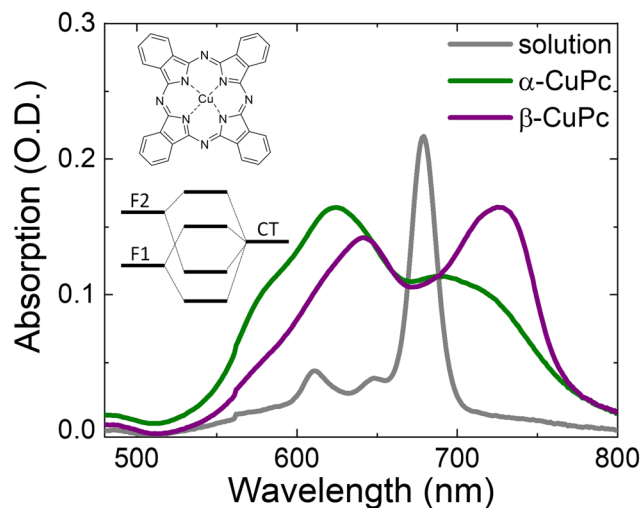
This journal is © the Owner Societies 2023

Phys. Chem. Chem. Phys., 2023, **25**, 6847–6856 | **6847**

Fig. 1 Steady-state absorption of CuPc in 1-chloronaphthalene solution and in thin films with α- and β-phase stacking morphologies in the spectral range of the Q-band absorption. The film samples exhibit different absorption peak positions and relative intensities due to changes in intermolecular couplings.

β-CuPc. Both morphologies are reported to exhibit Frenkel–CT mixing, but they also demonstrate differing steady-state optical properties. It remains unclear how the morphology influences the photoexcited dynamics of CuPc thin films. Differences in Frenkel–CT mixing, for example, could strongly alter the potential energy landscape.

Herein, we used transient absorption (pump–probe) spectroscopy to study the photophysical dynamics of α-CuPc and β-CuPc. Due to the intermolecular coupling interactions and Frenkel–CT mixing, the Q-band absorption of the thin films is much broader than that in solution (Fig. 1, *vide infra*). We characterized the photophysical dynamics at various excitation wavelengths across this Q-band absorption. We find that both α- and β-CuPc thin films exhibit ultrafast intersystem crossing to form CuPc triplet (T_1), as is seen in monomeric CuPc as well. However, we also find a unique excitation wavelength dependence in α-CuPc. At bluer excitation wavelengths, we observe a competitive decay pathway to a symmetry-breaking charge transfer photoproduct. We propose that the morphology dependence of our observations arises from differences in electronic and vibronic coupling in α- and β-CuPc.

Experimental

Sample preparation

CuPc [[29*H*, 31*H*, phthalycaninato(2-)-N29,N30,N31,N32) copper(II)] and 1-chloronaphthalene were purchased from Sigma-Aldrich and used without further purification.

The solution sample of CuPc was prepared by first heating the solvent to 60 °C and then adding the CuPc powder. This mixture was subsequently centrifuged and filtered to retrieve a homogenous solution. The final concentration gave an OD of 0.2 at 680 nm in a 2 mm cuvette.

For the thin film samples, quartz substrates (3 × 3 cm, 1 mm thick) were cleaned in an ultrasonic bath: 10 min. in acetone and 5 min in isopropyl alcohol. They were then dried under a N_2 gas flow. CuPc was vapor-deposited onto the quartz substrates under 10^{-6} mbar vacuum pressure, using a 0.1 Å s^{-1} deposition rate. The substrates were heated to and held at 150 °C during the deposition, and the thickness was monitored using a quartz crystal balance. This deposition resulted in α-CuPc thin films. In order to prepare β-CuPc samples, α-CuPc thin films were placed on a hot plate at 300 °C for 10 h.[63–66] The final CuPc layer thickness is 50.6 ± 0.8 nm, as determined by surface profilometry (Bruker, DektakXT). The assignment of α- and β-phase morphologies is consistent with the steady-state absorption from literature examples.[42,66,67]

Structural characterization

Grazing incidence wide-angle X-ray scattering (GIWAXS) measurements were performed at the Dortmund Electron Accelerator (DELTA) Synchrotron Facility (Dortmund, Germany), beamline BL09. The photon energy was set to be 10 keV ($\lambda = 1.24$ Å). The beam size was 1.0×0.2 mm^2 (width × height), and the samples were irradiated just below the critical angle for total reflection with respect to the incoming X-ray beam ($\sim 0.1°$). All X-ray scattering measurements were performed under vacuum (~ 1 mbar) to reduce air scattering and beam damage to the sample. All data processing and analyses were performed using the software package Datasqueeze.

Optical spectroscopy

Steady-state absorption was performed using a PerkinElmer Lambda900 spectrophotometer. Transient absorption (TA) spectroscopy was performed using a Helios-Fire pump–probe setup (Ultrafast Systems). This is paired with a regeneratively amplified 1030 nm laser (Light Conversion Pharos, 200 fs, 200 μJ), set at an effective repetition rate of 1 kHz *via* an internal pulse picker. A small portion (20%) of the 1030 nm fundamental is directed to an optical delay line, and, subsequently, to a sapphire crystal to generate the broadband probe light. The remaining 80% of the 1030 nm fundamental is directed to an optical parametric amplifier (Light Conversion, Orpheus-F) to generate the pump pulse at various wavelengths, as detailed further in the Results section. The pump excitation density at the sample was adjusted with a neutral density filter, and the beam diameter was measured using a LaserCamHR-II beam profiler (Coherent). Excitation density calculations are further detailed in the ESI.† Film samples were photoexcited from the backside of the sample to minimize pump scatter light entering the detector. Solution samples for TA were measured in a 2 mm cuvette with stirring, and in this case both pump and probe beams were directed onto the front face of the cuvette to minimize temporal dispersion. The relative polarization between the pump and probe beams was set to 54.7° (magic angle) to avoid anisotropic effects in the solution measurements. Global analysis[68] of TA data was performed using the R-package TIMP software,[69] with the graphical interface Glotaran 1.5.1.[70]

6848 | *Phys. Chem. Chem. Phys.*, 2023, **25**, 6847–6856

This journal is © the Owner Societies 2023

Results and discussion

Frenkel exciton and charge transfer mixing in CuPc films

Fig. 1 shows the steady-state absorption spectrum of CuPc in 1-chloronaphthalene solution as well as in thin films with predominantly α- and β-type morphology. The depicted spectral range between 500 and 800 nm shows the Q-band absorption region (S$_0$ → S$_1$) and agrees with literature examples.[67,71,72]

The solution sample represents the absorption of monomeric CuPc, which is characterized by a primary 0–0 transition at 680 nm, and two vibronic peaks at 620 and 645 nm. A single predominant 0–0 transition is expected for metallated phthalocyanines, due to the symmetric molecular geometry.[71] The absorption spectra of both α-CuPc and β-CuPc films are broader than that in solution, and each exhibit two predominant peaks. This splitting of the absorption band is due to excitonic splitting between strongly interacting dimers in the film.[13,73] The relative peak ratios differ between the two morphologies, as has been previously reported, and are consistent with changes in neighbor-to-neighbor molecular orientation. The structural organization of the thin films was measured using grazing-incidence wide-angle X-ray scattering (Fig. S1, ESI†). These experiments show that the α-CuPc exhibits a characteristic herringbone structure, while the β-CuPc film is polymorphic, but with clear evidence of larger molecular displacement between neighboring molecules within the stacks in the co-existing β-phase. The predominance of the blue (higher energy) peak in α-CuPc can be attributed to a more face-to-face π-stacking arrangement and thus stronger intermolecular coupling, while β-CuPc exhibits a more slip-stacked arrangement, consistent with a red (lower energy) shift.[66,74–76] More details on the GIWAXS measurements and analysis can be found in the ESI.†

In addition to excitonic splitting due to interacting dimers, the steady-state absorption in the solid state represents a mixed contribution between molecular excitons and a charge-transfer state which runs parallel to the π-stacking direction. In α-CuPc, the peaks at 625 and 690 nm are assigned to the first and second π–π* transitions on the phthalocyanine macrocycle, respectively, which represent the two lowest energy Frenkel excitons (F1, F2).[77,78] The Q-band absorption in α-CuPc also exhibits two shoulders at ∼580 and 725 nm, which arise as a result of excitonic mixing with an intermolecular CT state.[37,38] The absorption spectrum is therefore comprised of four overlapping peaks, representing a mixture of the two lowest energy intramolecular Frenkel excitons in CuPc (F1, F2) with an intermolecular charge-transfer state (CT), which is oriented through the crystalline stack (Fig. 1). The presence of such an intermolecular charge-transfer state coupled to the intramolecular Frenkel excitons has been identified in both α-CuPc and β-CuPc.[36,40,42,79–81] The spectral lineshape for the β-CuPc steady-state absorption can therefore be similarly explained, with the predominant peaks at 640 and 725 nm being assigned to the first and second π–π* transitions on the phthalocyanine macrocycle, and lower intensity shoulders contributing due to the four-fold (F1, F2)-CT mixing. In the

following, we explore how this mixing mediates photophysical dynamics in α- and β-CuPc.

Ultrafast intersystem crossing in monomeric CuPc

Fig. 2a shows TA spectra (λ_{ex} = 670 nm) of monomeric CuPc, measured in 1-chloronapthalene solution. The spectra exhibit negative features at 620, 645, and 680 nm, matching the peaks from steady-state absorption (overlaid in grey), which are attributed to ground-state bleaching (GSB). The CuPc solution TA spectra also exhibit broad positive features between 480–600 nm, attributed to excited state absorption (ESA). As the zoomed-in section in the inset of Fig. 2a shows, there is an increase in the ESA below 500 nm within the first 5 ps (blue to green traces). The solution TA data were fit using a two-compartment sequential global analysis model, and the resulting evolution associated difference spectra (EADS) are shown in Fig. 2b. The black trace represents the first EADS and corresponds to features appearing immediately after photoexcitation. In addition to the GSB features previously noted, there is also a negative contribution to the differential absorption spectrum at ∼725 nm and a broad ESA from 525–850 nm, which overlaps the negative features. This evolves in 340 fs to the second EADS (red), wherein the GSB features persist, but
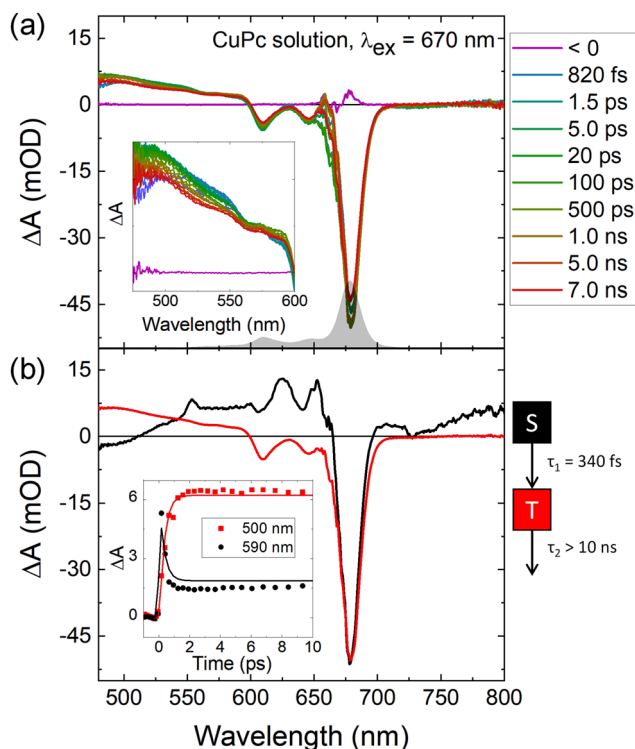

Fig. 2 (a) TA spectra at selected time delays of CuPc in 1-chloro-naphthalene photoexcited at λ_{ex} = 670 nm. Inset shows a zoom in of the ESA features between 480–600 nm, which blue-shift in the first few traces. The steady-state absorption profile of CuPc in 1-chloro-naphthalene from Fig. 1 is overlaid for comparison. (b) EADS from global analysis of the TA data, fit to a sequential two compartment scheme consistent with ultrafast intersystem crossing to a long-lived triplet state. Inset shows transient kinetics and fits comparing the decay of the singlet ESA at 590 nm and growth of the triplet ESA at 500 nm.

This journal is © the Owner Societies 2023

Phys. Chem. Chem. Phys., 2023, **25**, 6847–6856 | **6849**

the negative feature at 725 nm has disappeared. Furthermore, the ESA has blue-shifted and now shows a predominant peak at 500 nm. The transient kinetics within the first 10 ps are shown in the inset of Fig. 2b along with the fits from global analysis and confirm that the ESA at 590 nm disappears concomitantly with the rise of the ESA at 500 nm. This second EADS lives beyond the 8 ns measurement window of our experiment.

In order to describe the photophysics of monomeric CuPc and these EADS, we refer to earlier literature reports of inter-system crossing (ISC) in phthalocyanines.[82–87] CuPc in solution has previously been shown to exhibit no measurable fluorescence, but does exhibit phosphorescence.[88–90] The first EADS is therefore assigned to the population of the singlet excited state, S_1, and this further agrees with previously reported TA of ZnPc in solution.[85] The slight negative dip in the first EADS at 725 nm is attributed to a vibronic transition of the stimulated emission, based on the agreement with previous reports of CuPc fluorescence measured *via* upconversion.[91,92] The singlet excited state then undergoes ISC within 340 fs to yield the triplet excited state (T_1), represented by the second EADS. This assignment is consistent with the disappearance of the SE band as well as the long lifetime (>10 ns). The T_1 ESA lineshape also agrees with earlier flash-photolysis measurements, which further show that the CuPc triplet in solution has a lifetime of 35 ns.[82]

Excitation wavelength dependent TA of CuPc thin films

TA experiments for both α-CuPc and β-CuPc thin films were carried out using various excitation wavelengths across the Q-band absorption, chosen to approximately coincide with the energies of the four-fold mixed (F1, F2)-CT states. These

data are shown as contour plots in Fig. 3a–d and 4a–d for the full temporal measurement window, out to 7 ns. The excitation power at the sample was adjusted to maintain approximately equal excitation density at all of the pump wavelengths (Tables S1 and S2, ESI†).

In α-CuPc, (Fig. 3) all contour plots show positive features between 480 and 550 nm, and negative features between 600 and 750 nm. There is also a strong negative contribution between 560 and 580 nm, which appears with the highest relative intensity at λ_{ex} = 580 nm (red arrow, Fig. 3a) and has a diminishing contribution as the excitation energy shifts to longer wavelengths. The β-CuPc contour plots (Fig. 4) show positive features between 480 and 600 nm and at 700 nm, with negative contributions between 600 and 650 and 725 and 800 nm. In contrast to the α-CuPc sample, there are no obvious excitation wavelength dependent differences in the β-CuPc sample from the contour plots.

In order to elucidate excitation dynamics, we used global analysis to fit the TA data. The data was truncated to the first 50 ps to avoid heating artefacts. TA experiments on thin film samples are highly susceptible to local heating effects, and it is critical to avoid misinterpretation of a heat-induced spectral feature as a photoproduct.[93,94] Excitation density dependent measurements reveal the line shape which arises from local heating in α- and β-CuPc (Fig. S2, ESI†). Spectral traces of the TA data at selected pump–probe delay times indicate that the heating effects in these thin films appear only at longer timescales (Fig. S3, ESI†), in agreement with the literature.[83,93] We therefore limit the global analysis to the first 50 ps of the experiment window, where we are confident that heating
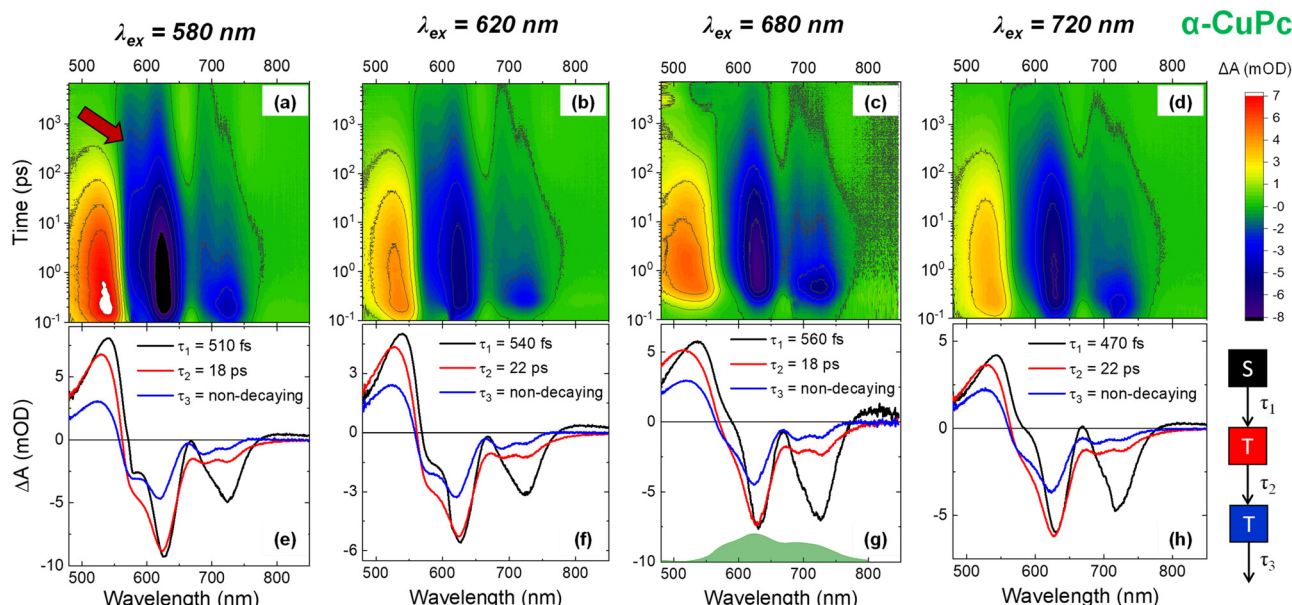

Fig. 3 (a–d) Contour plots of the TA measurements carried out on α-CuPc thin films photoexcited at various wavelengths across the Q-band absorption. For each sample, the excitation density was scaled to be similar at all excitation wavelengths. Red arrow: α-CuPc shows a negative band at 575 nm (red arrow) which is strongest at λ_{ex} = 580 nm and has a diminishing contribution as the excitation energy is red-shifted. (e–h) EADS from global analysis of the first 50 ps also shows excitation wavelength dependent differences. The steady-state spectrum of the α-CuPc thin film from Fig. 1 is reproduced in (g) for lineshape comparison.
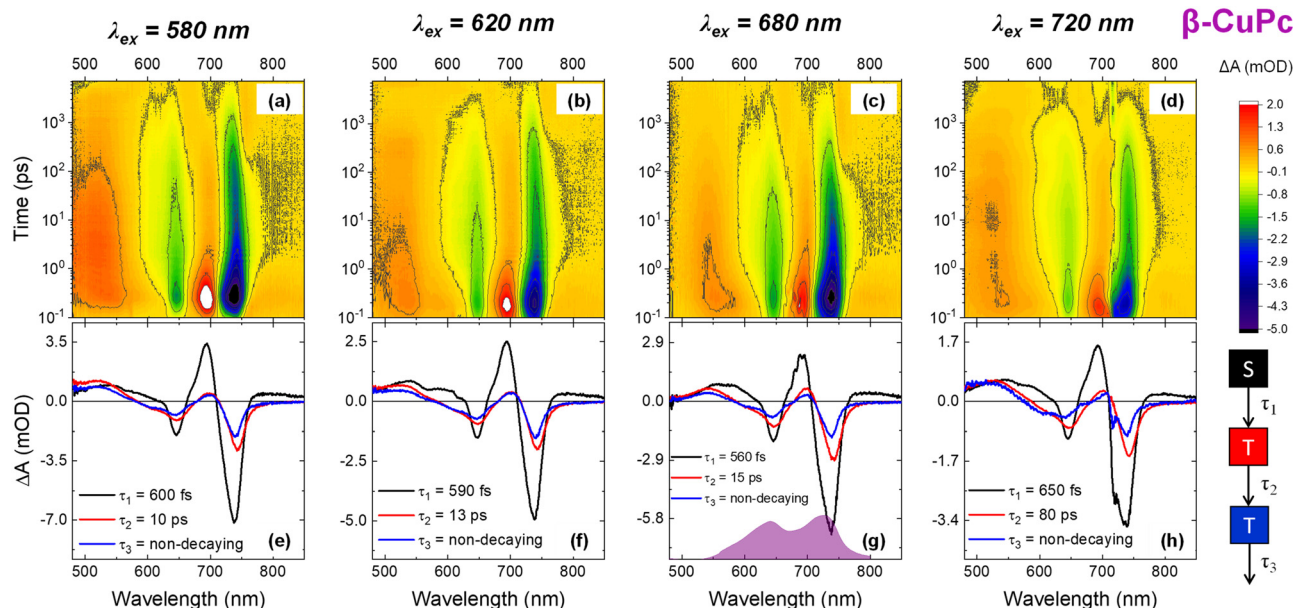
6850 | *Phys. Chem. Chem. Phys.*, 2023, **25**, 6847–6856

This journal is © the Owner Societies 2023

Fig. 4 (a–d) Contour plots of the TA measurements carried out on β-CuPc thin films photoexcited at various wavelengths across the Q-band absorption. The excitation density was scaled to be similar at all excitation wavelengths. No clear differences emerge based on excitation wavelength for β-CuPc. (e–h) EADS from global analysis of the first 50 ps also shows similar spectral lineshapes at all excitation wavelengths. The steady-state spectrum of the β-CuPc thin film from Fig. 1 is reproduced in (g) for lineshape comparison.

effects are minimal. The resulting EADS from global analysis of α-CuPc and β-CuPc TA data are shown in Fig. 3e–h and 4e–h, respectively. Datasets for both samples fit well to a sequential 3-compartment model, and each of these compartments will be further referred to as EADS 1, 2, 3, with specificity for the sample as EADS 1(α/β) when appropriate.

At all excitation wavelengths and in both samples, EADS 1 is attributed to the population of the singlet excited state. The positive features of EADS 1 are ascribed to S_1 absorption. In EADS 1α, the S_1 ESA appears as a broad feature from 480 to 550 nm with a peak at 545 nm. In EADS 1β, the S_1 ESA exhibits a broad peak from 480–600 nm and a strong absorption at 690 nm. The apparent differences are due to the differing interference with the sample GSB, but the general position of the S_1 ESA is the same for both α-CuPc and β-CuPc and also agrees with the solution S_1 ESA (Fig. 2b). The negative features of EADS 1 are characterized by a mix of GSB (550–750 nm) and SE (725 nm). In the case of EADS 1α, the SE exhibits a relatively larger intensity at longer excitation wavelengths, as compared with the GSB peak at 620 nm. In contrast, in EADS 1β, the relative intensity of the SE band compared to the GSB (640 nm) does not change with the excitation wavelength.

EADS 1 evolves into EADS 2 with the time constant τ_1 and, at all measured excitation wavelengths, this is accompanied by quenching of the SE. This is consistent with ISC from S_1 to T_1, with τ_1 representing the ISC rate. The consistent ISC rate of $\sim$500 fs for all samples agrees with the solution measurement. EADS 2 and EADS 3 have a similar line shape, suggesting that in the CuPc films the resulting T_1 decays biexponentially, with a faster rate on the order of $\sim$10 s of picoseconds and a slower rate on the order of nanoseconds. The faster decay is likely due

to annihilation effects in the crystalline thin films.[95] The slower decay is fixed as a non-decaying feature within this time window, but based on the full time range of data (Fig. S3, ESI†) we can approximate that T_1 fully recovers to the ground state on the order of nanoseconds, in agreement with literature.[83] The spectral evolution from EADS 1 to EADS 2 is accompanied by a blue-shift of the ESA, yielding a T_1 ESA with peak at $\sim$530 nm. This is in agreement with the T_1 ESA from solution (Fig. 2). In EADS2α, the quenched SE also reveals underlying GSB features, and the four GSB peaks in EADS2α correspond exactly to the two peaks and two shoulders from the steady-state absorption. As described above for Fig. 1, these arise from the (F1, F2)-CT mixing in the film. However, the two lower energy peaks are much smaller in ratio to the higher energy peaks when compared to the ground-state spectrum. This suggests the presence of an additional T_1 ESA between 675–800 nm, which is destructively interfering with the GSB in this region. Such an ESA is consistent with earlier literature reports on CuPc films,[96] as well as with EADS 2β which shows a positive feature at 700 nm. Similar to the GSB of EADS2α, EADS 2β shows multiple GSB peaks, consistent with (F1, F2)-CT mixing.

EADS 1/2/3β exhibit similar line shape at all excitation wavelengths. In contrast, EADS 1/2/3α have some distinct differences based on excitation wavelength. As has been mentioned above, the SE feature exhibits a higher relative intensity compared to the GSB with longer excitation wavelength. In addition, there is a negative feature between 560–580 nm, which appears strongest at shorter excitation wavelength, as expected from the contour plots. Furthermore, the relative intensity of the ESA in the 480–550 nm range is higher at shorter excitation wavelength. Fig. S4 (ESI†) compares the

spectral line shapes of the decay-associated difference spectra (DADS) for the fastest decay at each excitation wavelength, which indicate the spectral changes that occur with the associated decay time.[68,70] In the β-CuPc data, the line shapes are all similar and independent of excitation wavelength. However, in the α-CuPc data, the line shapes strongly differ in the range of 525–625 nm. Here, the α-CuPc DADS exhibit two peaks at 560 and 600 nm, and the peak ratios depend on the excitation wavelength. At λ_{ex} = 580, 620, the peak at 560 nm predominates, while at λ_{ex} = 680, 720, the peak at 600 nm is higher.

We highlight these differences further by comparing the transient kinetics at different excitation wavelengths for both α-CuPc and β-CuPc. Fig. 5 shows the transient kinetics monitored at select wavelengths. The transient kinetics at 725 nm (α-CuPc) and 740 nm (β-CuPc) depict the SE quenching followed by GSB decay, and therefore follow the ISC process. This is independent of excitation wavelength for both α-CuPc and β-CuPc, in agreement with literature.[83] As our solution measurements (Fig. 2) and earlier work[82] has shown, ISC in CuPc is intrinsic to the monomer, and occurs following excitation into the intramolecular Frenkel exciton plane.

However, the transient kinetics monitored at 560 nm show a marked dependence on excitation wavelength in α-CuPc. Here, the ΔA signal begins positive and then later becomes negative. As Fig. 5a shows, the rate of this change is faster for shorter excitation wavelengths. This is the same region associated with S_1 ESA decay and could point to a change in the rate of $S_1 \rightarrow T_1$. But, since the SE quenching does not exhibit the same dependence, this change is not due to the ISC. Instead, this observation suggests an additional photodynamic feature which appears differently depending on excitation wavelength.

Symmetry-breaking charge transfer in α-CuPc

Based on the contour plots, global analysis, and comparison of the transient kinetics, we conclude that the α-CuPc thin film
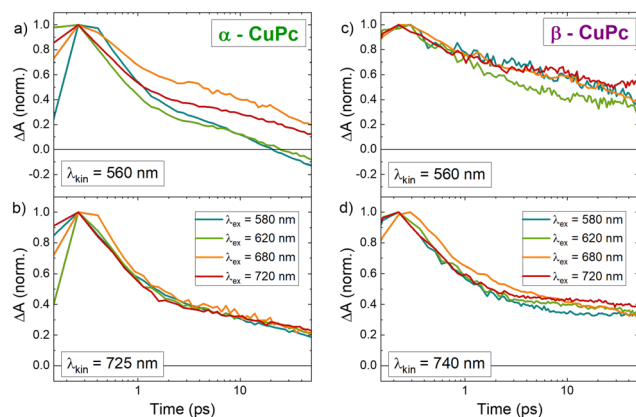

Fig. 6 Calculated difference spectrum between EADS fits for α-CuPc thin film excited at λ_{ex} = 580 nm and λ_{ex} = 720 nm shows features consistent with symmetry-breaking charge-transfer at λ_{ex} = 580 nm and increased relative stimulated emission at λ_{ex} = 720 nm.

exhibits a unique excitation wavelength dependence in its photophysics, described by an additional spectral feature around 560 nm. The question then remains to explain the origin of this feature in α-CuPc, and why it appears only in this morphology. Fig. 6 shows the difference spectrum ($\Delta\Delta A$) between λ_{ex} = 580 and λ_{ex} = 720, calculated for both EADS1α and EADS2α to highlight the excitation dependent changes. The $\Delta\Delta A$ spectra show a positive contribution between 480–550, with a peak at ~530 nm, a negative feature between 550–625 nm. ΔEADS1α also shows a positive feature at 725 nm.

We first consider if the excitation wavelength dependence could be a local heating artefact. Our own measurements and literature[83] report that local heating effects can produce a ΔA spectrum with a negative feature at 570 nm (Fig. S2, ESI†). However, the heating effects in these samples do not appear until after 100s of picoseconds, while the excitation wavelength dependent feature appears at very early times. In addition, the $\Delta\Delta A$ line shape in Fig. 6 also exhibits significant differences from the heating line shape. In particular the $\Delta\Delta A$ exhibits a positive feature in the region of 530 nm. We further confirm that this line shape is not due to local heating by comparing the spectral line shapes at λ_{ex} = 680 at different excitation densities (Fig. S5, ESI†). At delay times of 1 and 10 ps, the spectral line shapes match. We therefore conclude that the additional spectral feature in α-CuPc is not a heating effect.

The region at around 560–580 nm has also been identified as the spectral range where the intermolecular CT state exhibits a strong contribution in both α-CuPc and β-CuPc.[39,42,79–81] The excitation dependent feature identified in Fig. 6 furthermore agrees well with the published work reporting the cation spectrum measured for an α-CuPc thin film.[96] Recent work has also reported symmetry-breaking charge transfer and separation (SBCT) for a ZnPc dimer, and the spectral line shape of SBCT in that work matches closely with the $\Delta\Delta A$ spectrum in Fig. 6 of this work, albeit at a shifted spectral position due to

Fig. 5 Transient kinetics for (a and b) α-CuPc and (c and d) β-CuPc thin films show that at 560 nm, the α-CuPc decay dynamics vary with excitation wavelength. The decay dynamics of β-CuPc at 560 nm do not exhibit any such dependence. Furthermore, the kinetics associated with the SE quenching at 725 and 740 nm do not depend on excitation wavelength in either sample. Data truncated to the first 50 ps.
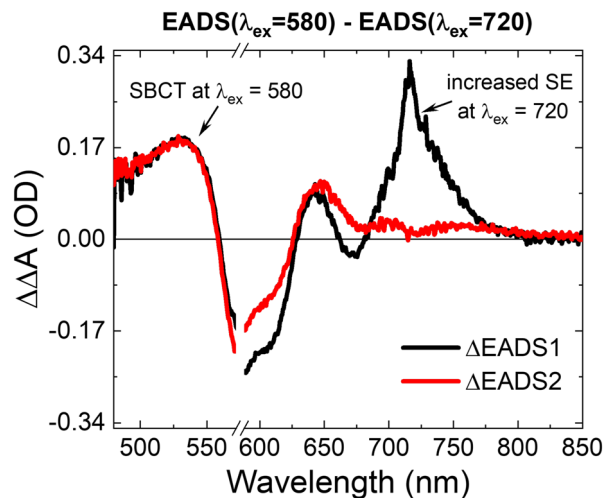
6852 | *Phys. Chem. Chem. Phys.*, 2023, **25**, 6847–6856

This journal is © the Owner Societies 2023

the shorter range coupling in the dimer.[97] Based on this evidence, we assign the ESA between 480–550 nm, which appears selectively at shorter-wavelength excitation, to SBCT through the α-CuPc stack. This feature is further accompanied by a GSB associated with the intermolecular CT band. In addition, the positive peak at 725 nm in ΔEADS1α is consistent with the earlier observation of a relatively higher degree of SE at longer excitation wavelengths.

Morphology dependence of mixed electronic pathways in CuPc

Our results point to the following picture for the excited state dynamics in CuPc solution and thin films (Fig. 7): in solution, the lowest Frenkel excitons F1, F2 are degenerate. Following excitation into the Frenkel exciton plane, ISC proceeds via a spin-exchange interaction between the Cu metal center and the π-ring ligands, which forms an intramolecular CT state in the molecule.[98–100] This offers an efficient pathway to ISC, without any spin–orbit coupling required.

In crystalline thin films, the degeneracy of the F1, F2 excitons is lifted, due to reduced symmetry. Since the ISC occurs intramolecularly, it is reasonable that this still occurs in the thin films.[83,101,102] Furthermore, the formation of the intermolecular CT state can also impact the photophysical pathways. As described in the text above, the multiple peaks associated with the steady-state absorption in α-CuPc and β-CuPc thin films arises from a mixture of the two lowest energy intramolecular Frenkel excitons in CuPc with an intermolecular charge-transfer state, which is oriented through the crystalline stack. The transition dipole moment of such a CT state will typically be small, but coupling to a Frenkel exciton can facilitate intensity borrowing, and allow for direct excitation into the CT state.[27,81] Photoexcitation of these crystalline thin film samples will lead to a coherent Frenkel/CT state, with varying character depending on electronic and vibrational coupling arising from the molecular packing.[20,103–105]

We therefore propose that in α-CuPc, longer wavelength excitation populates states with predominantly Frenkel (F1, F2) exciton character, yielding competitive SE and ISC, followed by triplet decay. Shorter wavelength excitation, on the other

hand, leads to multiple pathways in α-CuPc. Some of the excited state population still decays via SE + ISC. But another pathway also emerges, wherein excitation populates an excited state with significant CT character, resulting in the formation of a symmetry-breaking charge-transfer state, through the intermolecular stack. This is consistent with photocurrent measurements, which have indicated the formation of free charges in α-CuPc thin films upon direct excitation of the CT band.[80] These results also explain the reduced SE at shorter-wavelength excitation, as the excited state with significant CT character will not exhibit SE.

Previous work has reported SBCT in π-stacked MgPc and OTiPc, and in the latter case especially this was reported in various morphologies.[106,107] The contribution of a CT state to the absorption in the region of 560–570 nm is also present in β-CuPc.[41,42,79] But the sample with predominantly β-CuPc morphology exhibits no clear evidence of any excitation wavelength dependence from these experiments. In β-CuPc, our results suggest that a single pathway for ISC dominates, wherein excitation leads to excited states with predominately Frenkel exciton character, and subsequent ISC via the same spin-exchange mechanism as in the monomer.

The reason for selective SB-CT in α- vs. β-CuPc morphlogies can be attributed to both the differences in molecular packing as well as differences in vibronic coupling. The smaller Cu–Cu molecular packing distance in α-CuPc could lead to optimal electronic coupling for SBCT.[108,109] The GIWAXS measurements furthermore indicated that the β-CuPc thin film exhibits two phases, and this could have an impact on the disorder mediated photophysical decay pathways. Vibrational spectroscopy of SnPc showed that direct excitation of the CT is associated with intermolecular vibrational modes through the π-stacks.[103] Changes in vibronic coupling between the two morphologies can also be responsible for the observed photophysical differences. Previous work has shown that the CT state in α-CuPc is resonant with intramolecular vibrational energies in CuPc, but this does not hold for β-CuPc.[42,79] Vibronic coupling has been purported to facilitate and possibly accelerate SB-CT processes.[104] On the other hand, the vibronic spacing of the CT band in β-CuPc has also been shown to correlate with a vibrational mode associated with a pair of ionized CuPc molecules.[42] Therefore, another possibility is that the SBCT is occurring in β-CuPc, but remains more localized and recombines quickly. From the present experiments, it is not possible to distinguish between these two possibilities. However, the essential finding remains that α-CuPc and β-CuPc exhibit distinct photophysical behavior arising from the changes in vibronic as well as electronic coupling, which emerge due to the changes in morphology.
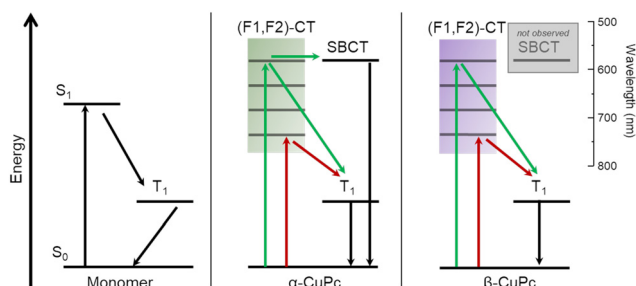

Fig. 7 Summary of photoexcited pathways in CuPc. The monomer exhibits ultrafast ISC followed by decay to the ground state. In α-CuPc and β-CuPc, the lowest excited states are spread over a broad range of energies due to the (F1, F2)-CT mixing. In α-CuPc, longer wavelength excitation leads to ISC, while shorter wavelength excitation leads to a competition between ISC and SBCT. In β-CuPc, only the ISC pathway is observed, independent of excitation wavelength (energies not to scale).

Conclusions

In this work, we have characterized the photophysical dynamics of the organic chromophore CuPc in solution and in two different solid-state morphologies, α-CuPc and β-CuPc. Transient absorption

This journal is © the Owner Societies 2023

Phys. Chem. Chem. Phys., 2023, **25**, 6847–6856 | **6853**

spectroscopy characterizes intramolecular ultrafast intersystem crossing (ISC) in CuPc in solution, which also occurs in the thin film. Our results further show an additional photodynamic feature in the transient spectra of α-CuPc, the appearance of which is furthermore excitation wavelength dependent. We identify this additional photoproduct as a symmetry-breaking charge transfer through the α-CuPc stack, which appears selectively upon excitation into the intermolecular CT band. Direct excitation of this intermolecular CT band is made possible by the strong mixing and resultant intensity borrowing to the Frenkel exciton manifold. The differences in molecular packing and spacing in α-CuPc and β-CuPc lead to differences in electronic and vibrational coupling, and this is why the SBCT state is only observed in the α-CuPc thin film.

These results suggest how intermolecular coupling and morphology mediate competitive photophysical pathways in organic chromophore systems, and could be used to design organic materials with selective pathways along mixed electronic states.

Author contributions

CR and ER designed the study and carried out data analysis and interpretation; ER and OY prepared the samples; ER carried out the optical spectroscopy experiments; OY, WP, and TM carried out the GIWAXS experiments, data analysis, and interpretation; CR and PB supervised the study; and ER, CR, and PB wrote the manuscript.

Conflicts of interest

There are no conflicts to declare.

Acknowledgements

Notes and references

1 C. W. Tang, *Appl. Phys. Lett.*, 1986, **48**, 183–185.
2 B. Kippelen and J.-L. Bredas, *Energy Environ. Sci.*, 2009, **2**, 251–261.
3 M. R. Wasielewski, *Acc. Chem. Res.*, 2009, **42**, 1910–1921.
4 D. Gust, *Adv. Bot. Res.*, 2016, **79**, 1–42.
5 M. R. Andersson, G. Yu and A. J. Heeger, *Synth. Met.*, 1997, **85**, 1275–1276.
6 J. H. Burroughes, D. D. C. Bradley, A. R. Brown, R. N. Marks, K. Mackay, R. H. Friend, P. L. Burns and A. B. Holmes, *Nature*, 1990, **347**, 539–541.
7 K. Goushi, K. Yoshida, K. Sato and C. Adachi, *Nat. Photonics*, 2012, **6**, 253–258.
8 R. J. Chesterfield, J. C. McKeen, C. R. Newman, P. C. Ewbank, D. A. Da Silva Filho, J. L. Brédas, L. L. Miller, K. R. Mann and C. D. Frisbie, *J. Phys. Chem. B*, 2004, **108**, 19281–19292.
9 J. H. Oh, S. Liu, Z. Bao, R. Schmidt and F. Würthner, *Appl. Phys. Lett.*, 2007, **91**, 212107.
10 C. J. Bardeen, *MRS Bull.*, 2013, **38**, 65–71.
11 D. Bialas, E. Kirchner, M. I. S. Röhr and F. Würthner, *J. Am. Chem. Soc.*, 2021, **143**, 4500–4518.
12 A. Köhler and H. Bässler, *Electronic processes in organic semiconductors: An introduction*, Wiley-VCH Verlag GmbH & Co. KGaA, Weinheim, Germany, 2015.
13 M. Kasha, H. R. Rawls and M. A. El-Bayoumi, *Pure Appl. Chem.*, 1965, **11**, 371–392.
14 R. M. Hochstrasser and M. Kasha, *Photochem. Photobiol.*, 1964, **3**, 317–331.
15 E. G. McRae and M. Kasha, *J. Chem. Phys.*, 1958, **28**, 721–722.
16 A. S. Davydov, *Sov. Phys. Uspekhi*, 1964, **7**, 145–178.
17 E. F. Sheka, *Mol. Cryst. Liq. Cryst.*, 1975, **29**, 323–343.
18 A. Oleson, T. Zhu, I. S. Dunn, D. Bialas, Y. Bai, W. Zhang, M. Dai, D. R. Reichman, R. Tempelaar, L. Huang and F. C. Spano, *J. Phys. Chem. C*, 2019, **123**, 20567–20578.
19 N. J. Hestand and F. C. Spano, *Chem. Rev.*, 2018, **118**, 7069–7163.
20 N. J. Hestand and F. C. Spano, *Acc. Chem. Res.*, 2017, **50**, 341–350.
21 D. Beljonne, H. Yamagata, J.-L. Brédas, F. C. Spano and Y. Olivier, *Phys. Rev. Lett.*, 2013, **110**, 226402.
22 M. Hoffmann, Z. G. Soos and K. Leo, *Nonlinear Opt.*, 2006, **29**, 227–237.
23 K. Schmidt, *Phys. Lett. A*, 2002, **293**, 83–92.
24 B. S. Basel, J. Zirzlmeier, C. Hetzer, S. R. Reddy, B. T. Phelan, M. D. Krzyaniak, M. K. Volland, P. B. Coto, R. M. Young, T. Clark, M. Thoss, R. R. Tykwinski, M. R. Wasielewski and D. M. Guldi, *Chem*, 2018, **4**, 1092–1111.
25 N. J. Hestand, H. Yamagata, B. Xu, D. Sun, Y. Zhong, A. R. Harutyunyan, G. Chen, H. L. Dai, Y. Rao and F. C. Spano, *J. Phys. Chem. C*, 2015, **119**, 22137–22147.
26 D. Qi, H. Su, M. Bastjan, O. D. Jurchescu, T. M. Palstra, A. T. S. Wee, M. Rübhausen and A. Rusydi, *Appl. Phys. Lett.*, 2013, **103**, 113303.
27 L. Sebastian, G. Weiser and H. Bassler, *Chem. Phys.*, 1981, **61**, 125–135.
28 M. H. Hennessy, Z. G. Soos, R. A. Pascal and A. Girlando, *Chem. Phys.*, 1999, **245**, 199–212.
29 M. Hoffmann, K. Schmidt, T. Fritz, T. Hasche, V. M. Agranovich and K. Leo, *Chem. Phys.*, 2000, **258**, 73–96.
30 Y. Hong, J. Kim, W. Kim, C. Kaufmann, H. Kim, F. Würthner and D. Kim, *J. Am. Chem. Soc.*, 2020, **142**, 7845–7857.
31 A. Austin, N. J. Hestand, I. G. McKendry, C. Zhong, X. Zhu, M. J. Zdilla, F. C. Spano and J. M. Szarko, *J. Phys. Chem. Lett.*, 2017, **8**, 1118–1123.

6854 | *Phys. Chem. Chem. Phys.*, 2023, **25**, 6847–6856

This journal is © the Owner Societies 2023

32 N. J. Hestand and F. C. Spano, *J. Chem. Phys.*, 2015, **143**, 244707.

33 L. Gisslén and R. Scholz, *Phys. Rev. B: Condens. Matter Mater. Phys.*, 2009, **80**, 115309.

34 N. J. Hestand, C. Zheng, A. R. Penmetcha, B. Cona, J. A. Cody, F. C. Spano and C. J. Collison, *J. Phys. Chem. C*, 2015, **119**, 18964–18974.

35 F. Balzer, N. J. Hestand, J. Zablocki, G. Schnakenburg, A. Lützen and M. Schiek, *J. Phys. Chem. C*, 2022, **126**(32), 13802–13813.

36 L. P. Doctor, M. Naumann, F. Ziegs, B. Büchner, A. Popov and M. Knupfer, *J. Phys. Chem. C*, 2021, **125**, 12398–12404.

37 A. Popescu, R. A. Younts, B. Hoffman, T. McAfee, D. B. Dougherty, H. W. Ade, K. Gundogdu and I. V. Bondarev, *Nano Lett.*, 2017, **17**, 6056–6061.

38 I. V. Bondarev, A. Popescu, R. A. Younts, B. Hoffman, T. McAfee, D. B. Dougherty, K. Gundogdu and H. W. Ade, *Appl. Phys. Lett.*, 2016, **109**, 213302.

39 R. Pandey, A. P. Moon, J. A. Bender and S. T. Roberts, *J. Phys. Chem. Lett.*, 2016, **7**, 1060–1066.

40 M. Knupfer, T. Schwieger, H. Peisert and J. Fink, *Phys. Rev. B: Condens. Matter Mater. Phys.*, 2004, **69**, 165210.

41 M. Naumann and M. Knupfer, *J. Chem. Phys.*, 2018, **149**, 084704.

42 H. Yoshida, Y. Tokura and T. Koda, *Chem. Phys.*, 1986, **109**, 375–382.

43 S. Feng, Y. C. Wang, Y. Ke, W. Z. Liang and Y. Zhao, *J. Chem. Phys.*, 2020, **153**, 034116.

44 S. Feng, Y.-C. Wang, W. Liang and Y. Zhao, *Phys. Chem. Chem. Phys.*, 2022, **24**, 2974–2987.

45 M. A. Shaibat, L. B. Casabianca, D. Y. Siberio-Pérez, A. J. Matzger and Y. Ishii, *J. Phys. Chem. B*, 2010, **114**, 4400–4406.

46 P. Gregory, *J. Porphyrins Phthalocyanines*, 2000, **04**, 432–437.

47 A. Braz, M. López-López, G. Montalvo and C. G. Ruiz, *Aust. J. Forensic Sci.*, 2014, 1–10.

48 J. Danziger, P. Lee, K. W. Nebesny, N. R. Armstrong and J. P. Dodelet, *Chem. Mater.*, 1991, **3**, 821–829.

49 P. Peumans and S. R. Forrest, *Appl. Phys. Lett.*, 2001, **79**, 126–128.

50 G. J. Dutton and S. W. Robey, *J. Phys. Chem. C*, 2012, **116**, 19173–19181.

51 I. Kim, H. M. Haverinen, Z. Wang, S. Madakuni, Y. Kim, J. Li and G. E. Jabbour, *Chem. Mater.*, 2009, **21**, 4256–4260.

52 E. W. Snedden, A. P. Monkman and F. B. Dias, *Adv. Mater.*, 2013, **25**, 1930–1938.

53 T. Sasaki, K. Tabata, K. Tsukagoshi, A. Beckel, A. Lorke and Y. Yamamoto, *Thin Solid Films*, 2014, **562**, 467–470.

54 C.-H. Cheng, Z.-Q. Fan, S.-K. Yu, W.-H. Jiang, X. Wang, G.-T. Du, Y.-C. Chang and C.-Y. Ma, *Appl. Phys. Lett.*, 2006, **88**, 213505.

55 I. El Ouedghiri-Idrissi, M. Lougdali, Z. Makir, O. A. Niasse and Z. Sofiani, *Mater. Today Proc.*, 2022, **66**(1), 76–79.

56 N. Mutz, S. Park, T. Schultz, S. Sadofev, S. Dalglish, L. Reissig, N. Koch, E. J. W. List-Kratochvil and S. Blumstengel, *J. Phys. Chem. C*, 2020, **124**, 2837–2843.

57 N. Krishnan K, A. Sreedharan, S. Sagar, L. Thomas Manamel, A. Mukherjee and B. C. Das, *Appl. Surf. Sci.*, 2021, **568**, 150818.

58 G. R. Monama, K. D. Modibane, K. E. Ramohlola, K. M. Molapo, M. J. Hato, M. D. Makhafola, G. Mashao, S. B. Mdluli and E. I. Iwuoha, *Int. J. Hydrog. Energy*, 2019, **44**, 18891–18902.

59 J. Bian, L. Sun, Z. Zhang, Z. Li, M. Chu, X. Li, D. Tang and L. Jing, *ACS Sustain. Chem. Eng.*, 2021, **9**, 2400–2408.

60 L. Gui, J. Zhou, L. Zhou and S. Wei, *J. Mater. Chem. B*, 2018, **6**, 2078–2088.

61 H. Abramczyk and I. Szymczyk, *J. Mol. Liq.*, 2004, **110**, 51–56.

62 P. C. Lo, M. S. Rodríguez-Morgade, R. K. Pandey, D. K. P. Ng, T. Torres and F. Dumoulin, *Chem. Soc. Rev.*, 2020, **49**, 1041–1056.

63 G. Maggioni, A. Quaranta, S. Carturan, A. Patelli, M. Tonezzer, R. Ceccato and G. Della Mea, *Chem. Mater.*, 2005, **17**, 1895–1904.

64 S. Heutz, S. M. Bayliss, R. L. Middleton, G. Rumbles and T. S. Jones, *J. Phys. Chem. B*, 2000, **104**, 7124–7129.

65 O. Berger, W.-J. Fischer, B. Adolphi, S. Tierbach, V. Melev and J. Schreiber, *J. Mater. Sci.: Mater. Electron.*, 2000, **11**, 331–346.

66 J. Jungyoon, S. Kim, E. Lim, K. Lee, D. Cha and B. Friedman, *Appl. Surf. Sci.*, 2003, **205**, 274–279.

67 E. A. Lucia and F. D. Verderame, *J. Chem. Phys.*, 1968, **48**, 2674–2681.

68 I. H. M. Van Stokkum, D. S. Larsen and R. Van Grondelle, *Biochim. Biophys. Acta, Bioenerg.*, 2004, **1657**, 82–104.

69 K. M. Mullen and I. H. M. van Stokkum, *J. Stat. Softw.*, 2007, **18**, 1–46.

70 J. J. Snellenburg, S. Laptenok, R. Seger, K. M. Mullen and I. H. M. van Stokkum, *J. Stat. Softw.*, 2012, **49**, 1–22.

71 C. G. Claessens, U. Hahn and T. Torres, *Chem. Rec.*, 2008, **8**, 75–97.

72 J. H. Sharp and M. Abkowitz, *J. Phys. Chem.*, 1973, **77**, 477–481.

73 A. S. Davydov, *Uspekhi Fiz. Nauk*, 1964, **82**, 393–448.

74 T. Zou, X. Wang, H. Ju, L. Zhao, T. Guo, W. Wu, H. Wang, T. Zou, X. Wang, H. Ju, L. Zhao, T. Guo, W. Wu and H. Wang, *Crystals*, 2018, **8**, 22.

75 *Molecular Magnets: Physics and Applications*, ed. J. Bartolomé, F. Luis and J. F. Fernández, Springer Berlin Heidelberg, Berlin, Heidelberg, 2014.

76 X. F. Zhang, Q. Xi and J. Zhao, *J. Mater. Chem.*, 2010, **20**, 6726–6733.

77 M. M. El-Nahass, F. S. Bahabri, A. A. Al Ghamdi and S. R. Al-Harbi, *Egypt. J. Sol.*, 2002, **25**, 307–321.

78 A. T. Davidson, *J. Chem. Phys.*, 1982, **77**, 168–172.

79 Y. Tokura, T. Koda, Y. Iyechika and H. Kuroda, *Chem. Phys. Lett.*, 1983, **102**, 174–178.

80 N. Minami and M. Asai, *Jpn. J. Appl. Phys.*, 1987, **26**, 1754–1758.

81 A. Yadav, Y. Jin, P. K. L. Chan, M. Shtein and K. P. Pipe, *Appl. Phys. Lett.*, 2010, **97**, 203307.

This journal is © the Owner Societies 2023

Phys. Chem. Chem. Phys., 2023, **25**, 6847–6856 | **6855**

82 J. McVie, R. S. Sinclair and T. G. Truscott, *J. Chem. Soc., Faraday Trans. 2*, 1978, **74**, 1870–1879.

83 B. W. Caplins, T. K. Mullenbach, R. J. Holmes and D. A. Blank, *Phys. Chem. Chem. Phys.*, 2016, **18**, 11454–11459.

84 D. Frackowiak, A. Planner, A. Waszkowiak, A. Boguta, R. M. Ion and K. Wiktorowicz, *J. Photochem. Photobiol., A*, 2001, **141**, 101–108.

85 J. Savolainen, D. van der Linden, N. Dijkhuizen and J. L. Herek, *J. Photochem. Photobiol., A*, 2008, **196**, 99–105.

86 T. H. Tran-Thi, J. F. Lipskier, D. Houde, C. Pépin, E. Keszei and J. P. Jay-Gerin, *J. Chem. Soc., Faraday Trans.*, 1992, **88**, 2129–2137.

87 A. V. Nikolaitchik, *J. Phys. Chem. A*, 1999, **103**, 7587–7596.

88 D. Eastwood, L. Edwards, M. Gouterman and J. Steinfeld, *J. Mol. Spectrosc.*, 1966, **20**, 381–390.

89 P. S. Vincett, E. M. Voigt and K. E. Rieckhoff, *J. Chem. Phys.*, 1971, **55**, 4127–4131.

90 K. Yoshino, M. Hikida, K. Tatsuno, K. Kaneto and Y. Inuishi, *J. Phys. Soc. Jpn.*, 1973, **34**, 441–445.

91 T. Uemura, M. Furumoto, T. Nakano, M. Akai-Kasaya, A. Saito, M. Aono and Y. Kuwahara, *Chem. Phys. Lett.*, 2007, **448**, 232–236.

92 A. Okada, K. Kanazawa, K. Hayashi, N. Okawa, T. Kurita, O. Takeuchi and H. Shigekawa, *Appl. Phys. Express*, 2010, **3**, 015201.

93 S. Albert-Seifried and R. H. Friend, *Appl. Phys. Lett.*, 2011, **98**, 223304.

94 M. Ichikawa, H. Fukumura and H. Masuhara, *J. Phys. Chem.*, 1994, **98**, 12211–12214.

95 Y. Z. Ma, K. Xiao and R. W. Shaw, *J. Phys. Chem. C*, 2012, **116**, 21588–21593.

96 S. Padgaonkar, S. H. Amsterdam, H. Bergeron, K. Su, T. J. Marks, M. C. Hersam and E. A. Weiss, *J. Phys. Chem. C*, 2019, **123**, 13337–13343.

97 M. Cacioppo, T. Scharl, L. Đorđević, A. Cadranel, F. Arcudi, D. M. Guldi and M. Prato, *Angew. Chem., Int. Ed.*, 2020, **59**, 12779–12784.

98 M. S. Liao and S. Scheiner, *J. Chem. Phys.*, 2001, **114**, 9780–9791.

99 M. H. Ha-Thi, N. Shafizadeh, L. Poisson and B. Soep, *J. Phys. Chem. A*, 2013, **117**, 8111–8118.

100 W. Wu, *J. Chem. Phys.*, 2014, **140**, 224301.

101 L. Lozzi, S. Santucci, S. La Rosa, B. Delley and S. Picozzi, *J. Chem. Phys.*, 2004, **121**, 1883–1889.

102 B. W. Caplins, T. K. Mullenbach, R. J. Holmes and D. A. Blank, *J. Phys. Chem. C*, 2015, **119**, 27340–27347.

103 M. Hirasawa, Y. Sakazaki, H. Hane and T. Kobayashi, *Chem. Phys. Lett.*, 2004, **392**, 390–395.

104 C. Lin, T. Kim, J. D. Schultz, R. M. Young and M. R. Wasielewski, *Nat. Chem.*, 2022, **2022**, 1–8.

105 R. M. Young and M. R. Wasielewski, *Acc. Chem. Res.*, 2020, **53**, 1957–1968.

106 M. Tsushima, N. Ikeda, H. Yonehara, H. Etori, C. Pac and T. Ohno, *Coord. Chem. Rev.*, 2002, **229**, 3–8.

107 J. Mi, L. Guo, Y. Liu, W. Liu, G. You and S. Qian, *Phys. Lett. A: Gen. At. Solid State Phys.*, 2003, **310**, 486–492.

108 A. Aster, G. Licari, F. Zinna, E. Brun, T. Kumpulainen, E. Tajkhorshid, J. Lacour and E. Vauthey, *Chem. Sci.*, 2019, **10**, 10629–10639.

109 E. Sebastian and M. Hariharan, *ACS Energy Lett.*, 2022, **44**, 696–711.

6856 | *Phys. Chem. Chem. Phys.*, 2023, **25**, 6847–6856

This journal is © the Owner Societies 2023